

Separated twins or just siblings? A multi-planet system around an M dwarf including a cool sub-Neptune

MALLORY HARRIS,¹ DIANA DRAGOMIR,¹ ISMAEL MIRELES,¹ KAREN A. COLLINS,² SOLÈNE ULMER-MOLL,^{3,4} STEVE B. HOWELL,⁵ KEIVAN G. STASSUN,⁶ GEORGE ZHOU,⁷ CARL ZIEGLER,⁸ FRANÇOIS BOUCHY,³ CÉSAR BRICEÑO,⁹ DAVID CHARBONNEAU,¹⁰ KEVIN I. COLLINS,¹¹ GÁBOR FÜÜRÉSZ,¹² NATALIA M. GUERRERO,^{13,12} JON M. JENKINS,⁵ ERIC L. N. JENSEN,¹⁴ MARTTI H. K. KRISTIANSEN,¹⁵ NICHOLAS LAW,¹⁶ MONIKA LENDL,³ ANDREW W. MANN,¹⁶ HUGH P. OSBORN,^{4,12} SAMUEL N. QUINN,² GEORGE R. RICKER,¹² RICHARD P. SCHWARZ,² SARA SEAGER,^{17,12,18} ERIC B. TING,⁵ ROLAND VANDERSPEK,¹² DAVID WATANABE,¹⁹ AND JOSHUA N. WINN²⁰

¹Department of Physics and Astronomy, University of New Mexico, Albuquerque, NM, USA

²Center for Astrophysics | Harvard & Smithsonian, 60 Garden Street, Cambridge, MA 02138, USA

³Observatoire de Genève, Université de Genève, Chemin Pegasi 51, CH-1290 Sauverny, Switzerland

⁴Physikalisches Institut, University of Bern, Gesellschaftsstrasse 6, 3012 Bern, Switzerland

⁵NASA Ames Research Center, Moffett Field, CA 94035, USA

⁶Department of Physics and Astronomy, Vanderbilt University, Nashville, TN 37235, USA

⁷Centre for Astrophysics | University of Southern Queensland, Toowoomba, QLD, AU

⁸Department of Physics, Engineering and Astronomy, Stephen F. Austin State University, 1936 North St, Nacogdoches, TX 75962, USA

⁹Cerro Tololo Inter-American Observatory, Casilla 603, La Serena, Chile

¹⁰Harvard-Smithsonian Center for Astrophysics, 60 Garden St, Cambridge, MA 02138, USA

¹¹George Mason University, 4400 University Drive, Fairfax, VA, 22030 USA

¹²Department of Physics and Kavli Institute for Astrophysics and Space Research, Massachusetts Institute of Technology, Cambridge, MA 02139, USA

¹³Department of Astronomy, University of Florida, Gainesville, FL, 32611, USA

¹⁴Department of Physics & Astronomy, Swarthmore College, Swarthmore PA 19081, USA

¹⁵Brorfelde Observatory, Observator Gyldenkerne Vej 7, DK-4340 Tølløse, Denmark

¹⁶Department of Physics and Astronomy, The University of North Carolina at Chapel Hill, Chapel Hill, NC 27599-3255, USA

¹⁷Department of Earth, Atmospheric, and Planetary Sciences, Massachusetts Institute of Technology, Cambridge, MA 02139, USA

¹⁸Department of Aeronautics and Astronautics, Massachusetts Institute of Technology, Cambridge, MA 02139, USA

¹⁹Planetary Discoveries, Fredericksburg, VA 22405, USA

²⁰Department of Astrophysical Sciences, Princeton University, Princeton, NJ 08544, USA

ABSTRACT

We report the discovery of two *TESS* sub-Neptunes orbiting the early M dwarf TOI-904 (TIC 261257684). Both exoplanets, TOI-904 b and c, were initially observed in *TESS* sector 12 with twin sizes of $2.49R_{\oplus}$ and $2.31R_{\oplus}$, respectively. Through observations in five additional sectors in the *TESS* primary mission and the first and second extended missions, the orbital periods of both planets were measured to be 10.887 ± 0.001 and 83.999 ± 0.001 days, respectively. Reconnaissance radial velocity measurements (taken with EULER/CORALIE) and high resolution speckle imaging with adaptive optics (obtained from SOAR/HRCAM and Gemini South/ZORRO) show no evidence of an eclipsing binary or a nearby companion, which together with the low false positive probabilities calculated with the statistical validation software TRICERATOPS establish the planetary nature of these candidates. The outer planet, TOI-904 c, is the longest-period M dwarf exoplanet found by *TESS*, with an estimated equilibrium temperature of 217K. As the three other validated planets with comparable host stars and orbital periods were observed by Kepler around much dimmer stars ($J_{mag} > 12$), TOI-904 c, orbiting a brighter star ($J_{mag} = 9.6$), is the coldest M dwarf planet easily accessible for atmospheric follow-up. Future mass measurements and transmission spectroscopy of the similar sized planets in this system could determine whether they are also similar in density and composition, suggesting a common formation pathway, or whether they have distinct origins.

1. INTRODUCTION

The past decade of exoplanet exploration has revealed that M dwarf stars typically host multiplanet systems of small, rocky planets with orbital periods $P < 20$ days (Dressing & Charbonneau 2015; Hardegree-Ullman et al. 2019). As these cool, low-mass stars allow for easier detections and characterizations of exoplanets than larger hosts, whether via deeper transits or more significant radial velocity reflex motion, these short-period planets have been prioritized for in-depth study by the exoplanet community. Yet few planets have been found at greater distances from M dwarf hosts to date. Indeed, the *Kepler* mission only discovered ~ 30 M dwarf planets at distances > 0.15 AU (periods $P > 25$ days) (Muirhead et al. 2012; Barclay et al. 2015; Torres et al. 2015; Dressing & Charbonneau 2015; Morton et al. 2016; Torres et al. 2017; Berger et al. 2018), all of which orbit stars dimmer than $V_{\text{mag}}=15$ and thus are not easily accessible for ground-based observations. By prioritizing M dwarf stars and focusing on stars in the solar neighborhood, the Transiting Exoplanet Survey Satellite (*TESS*) now has the potential to populate this under-explored region of parameter space and provide targets for future characterization.

TESS is conducting a full-sky survey of nearby, bright stars, 75% of which are M dwarfs (Ricker et al. 2015). Unlike *Kepler*, which observed one region of the sky for four years, the *TESS* primary mission observed both hemispheres by cycling through 26 sectors observed for ~ 27 day intervals, and it is continuing to re-observe the hemispheres (as well as the ecliptic) in the same fashion through its extended missions. While this observation strategy makes *TESS* most sensitive to planets with $P \lesssim 10$ days, there exists the potential to observe planets with longer orbital periods in overlapping sectors near the ecliptic poles. Further, *TESS* is projected to observe many planets with $P \gtrsim 25$ days as single-transit events (Villanueva et al. 2019) that could be recovered in later extended missions. Since its launch in 2018, *TESS* has found 28 confirmed planets with periods > 25 days, 5 of which (Cañas et al. 2020; Rodriguez et al. 2020; Fukui et al. 2022; Mann et al. 2022; Schanche et al. 2022) orbit low-mass stars.

In this Letter, we introduce and statistically validate *TESS* Object of Interest (TOI) 904 c, a sub-Neptune with a period of 84 days that was observed to produce a single transit event in four different sectors of the *TESS* primary mission and its first and second extended missions. We also introduce another planet in the same system (TOI-904 b) with a period of 10.87 days. Orbiting an early M dwarf (TIC 261257684, TOI-904) at $T_{\text{equil}} \approx 200\text{K}$, TOI-904 c is the coldest M dwarf planet

discovered by *TESS* to date. Only three other transiting planets have been observed around low-mass stars with similar orbital periods: Kepler-186 f ($P=129.94$ days; Quintana et al. 2014), Kepler-1229 b ($P=86.83$ days; Morton et al. 2016) and Kepler-1628 b ($P=76.38$ days; Morton et al. 2016). Unlike these planets, TOI-904 c orbits an M dwarf bright enough ($J_{\text{mag}} = 9.61$) for future mass measurements and atmospheric characterization. Through these additional observations, this system embodies a (currently) unique opportunity to test theories of planet formation around low-mass stars. Further, by measuring the densities and constraining the composition of both planets in this system, we can determine whether these similarly sized planets also have twin compositions and formation histories, or if they evolved through distinct formation pathways while orbiting the same host star.

2. OBSERVATIONS

2.1. *TESS* Observations

TESS observed TOI-904 in Sectors 12 and 13 (2019 May 21 to 2019 July 17) of its primary mission (PM), Sectors 27, 38 and 39 (2020 July 05 to 2020 July 30, 2021 April 29 to 2021 June 24) of its first extended mission (EM1) and Sector 61 (2023 January 18 to 2023 February 12) of its second extended mission (EM2). TOI-904 was included in the *TESS* Candidate Target List (Stassun et al. 2019) and was monitored in both the 2-minute postage stamps (PS) and longer cadence (30-minutes in PM, 10-minutes in EM1, 200-seconds in EM2) Full-Frame Images (FFI) during both missions (see Fig. 1). The transit signatures of TOI-904 b and c were initially detected by the Science Processing Operations Center, (SPOC; Jenkins et al. 2016) located at the NASA Ames Research Center, in a transit search of Sector 12 with a noise-compensating matched filter (Jenkins 2002; Jenkins et al. 2010, 2020) on 2019 July 01. This filter originally folded a single transit of TOI-904 c onto the second transit of TOI-904 b. Both the SPOC and the Visual Survey Group (VSG; Kristiansen et al. 2022) working in conjunction with the *TESS* Single Transit Planet Candidate Working Group (TSTPC) flagged these transit events and attributed both to a single planet candidate with an orbital period of 18.35 ± 0.005 days. The correct period of TOI-904 b, 10.877 ± 0.001 days, was identified by the SPOC via a transit search of Sector 13 conducted on 2019 July 27. The transit signature passed all the diagnostic tests presented in the resulting Data Validation report (Twicken et al. 2018) and was fitted with an initial limb-darkened transit model (Li et al. 2019). The difference image centroiding test located the source of the transit signature to within 1.3 ± 2.9 arcsec. The

TESS Science Office reviewed the diagnostic results and issued an alert for TOI-904.01 on 2019 June 23 (Guerero et al. 2021), and it was then recognized as a *TESS* Object of Interest on 2019 July 15 on the *TESS* data alerts web portal at the Massachusetts Institute of Technology¹.

The SPOC conducted a subsequent multisector search of Sectors 12, 13, 27, 38 and 39 on 2021 July 25, where they recovered 12 transits of TOI-904 b and the signature of TOI-904 c at $4\times$ the true period (see Appendix B). The SPOC found the difference imaging centroiding test located the source of the transit signature to within 3.4 ± 3.4 arcsec. In August 2021, a member of the TSTPC working group (Hugh Osborn) found an undetected additional transit of TOI-904 c in SPOC-produced light curves near the end of *TESS* Sector 39, which together with the Sector 12 transit constrained the period of this planet to a discrete set of possible aliases. We proceeded to search all previous *TESS* observations of this star for additional transits of this outer planet, and discovered a third clear transit in *TESS* Sector 27 from which we were able to derive a unique period of 83.999 ± 0.001 days. This planet was registered as a community TOI on 2021 September 01, and the TESS Science Office issued an alert for it on 2022 April 20. We searched the *TESS* observations of TOI-904 for any additional transit signals and found no evidence of additional planets in this system from the transit method.

To investigate possible false positive scenarios of the planets that were observed in this system, we visually inspected the background of each individual light curve that included a transit of the outer planet to rule out false positives due to asteroids or other anomalies. We also used the Gaia DR3 (Gaia Collaboration et al. 2022) to investigate the possibility for blended objects in the aperture and whether the Re-normalised Unit Weight Error (RUWE), a measure of the normalized chi-square of the Gaia observations to the astrometric single-star fit corrected for color and magnitude dependencies (Lindgren et al. 2018; Pearce et al. 2020), indicated that the host star existed in a binary that could be responsible for the observed transits. With a RUWE metric ≈ 0.999 , TOI-904 showed no obvious indication of being a stellar binary (Pearce et al. 2020). As our preliminary inspection gave no indication that either planet candidates' transits were false positives, we looked to follow-up observations (as described in the following Sections) to further validate this system.

2.2. Ground-Based Photometry

The *TESS* pixel scale is $\sim 21''$ pixel⁻¹, and photometric apertures typically extend out to roughly 1 arcminute, which generally results in multiple stars blending in the *TESS* aperture. An eclipsing binary in one of the nearby blended stars could thus mimic a transit-like event in the large *TESS* aperture. With additional ground-based photometric observations, we can attempt to (1) rule out or identify nearby eclipsing binaries (NEBs) as potential sources of the detection in the *TESS* data, (2) check for the transit-like event on-target using smaller photometric apertures than in the *TESS* images to confirm that the event is occurring on-target, or in a star so close to TOI-904 that it was not detected by Gaia DR3 (which is unlikely as such a star would be too faint unless it is perfectly aligned with the target star, but which is accounted for in the *triceratops* transit probability calculation in Section 3.2), and (3) refine the *TESS* ephemeris.

2.2.1. Las Cumbres Observatory

We acquired ground-based transit follow-up photometry of TOI-904 b as part of the *TESS* Follow-up Observing Program Sub Group 1 (TFOP SG1; Collins 2019)². We used the TESS Transit Finder, which is a customized version of the *Tapir* software package (Jensen 2013), to schedule our transit observations and *AstroImageJ* (Collins et al. 2017) to extract differential photometry.

We observed predicted transit windows of TOI-904 b in Pan-STARRS *z*-short band from the Las Cumbres Observatory Global Telescope (LCOGT; Brown et al. 2013) 1.0 m network nodes at Siding Spring Observatory and South Africa Astronomical Observatory on UTC 2020 October 15 and 2020 December 19, respectively. The 1 m telescopes are equipped with 4096×4096 SINISTRO cameras having an image scale of $0''.389$ per pixel, resulting in a $26' \times 26'$ field of view. The images were calibrated by the standard LCOGT BANZAI pipeline (McCully et al. 2018).

We used circular photometric apertures of radius $1''.9$ and $5''.8$ to check for possible NEBs that could be contaminating the SPOC photometric apertures, which generally extend $\sim 1'$ from the target star. To account for possible contamination from the wings of neighboring star PSFs, we searched for NEBs in all known Gaia EDR3 and TIC version 8 nearby stars out to $2'.5$ from TOI-904 that are possibly bright enough in *TESS* band to produce the *TESS* detection (assuming a 100%

¹ <https://doi.org/10.17909/t9-wx1n-aw08>

² <https://tess.mit.edu/followup>

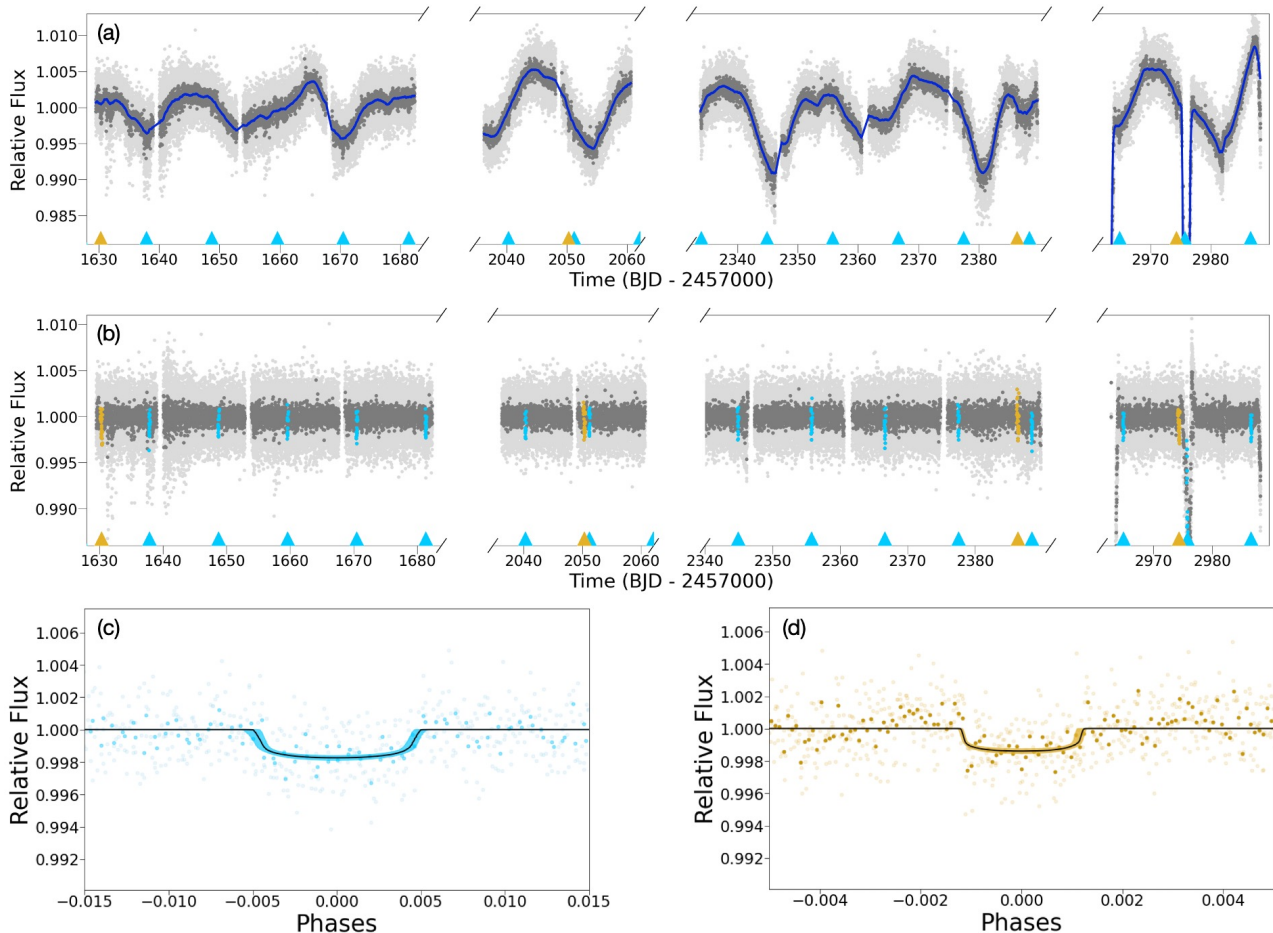


Figure 1. TESS observations of TOI-904. **Panel (a):** Raw observations of each *TESS* sector, with 2-minute data shown in light grey and 10-minute binned data shown in dark grey. We show the Tukey biweight trend calculated with the *wotan* (Hippke et al. 2019) library of the variability is shown in dark blue. Each planet transit is denoted by an arrow at the bottom of the graph, with blue denoting transits of TOI-904 b and gold denoting transits TOI-904 c. **Panel (b):** TESS data detrended by the same fit, with each transit high-lighted in the same color as the arrows in the previous figure. **Panel (c):** The phase folded light curves of transits of TOI-904 b with the transit fit including a shaded region denoting 1σ uncertainty. **Panel (d):** The phase-folded light curves of TOI-904 c with the transit fit including a shaded region denoting 1σ uncertainty.

eclipse and 100% contamination of the *TESS* aperture). To attempt to account for possible delta-magnitude differences between *TESS*-band and the follow-up Pan-STARRS *z*-short band, we checked stars that are an extra 0.5 magnitudes fainter in *TESS*-band than needed. We consider a star cleared of an NEB if the RMS of its 10-minute binned light curve is more than a factor of 5 smaller than the adjusted expected NEB depth in the star (adjusted to allow for the potential *TESS*-band delta-magnitude difference). We then visually inspect each neighboring star’s light curve to ensure no obvious eclipse-like signal. The NEB check light curve data are available at ExoFOP-*TESS*³. We rule out an NEB as the source of the TOI-904 b signal in the *TESS* data.

Photometry of TOI-904 was extracted using circular apertures with radius $5''.8$, which exclude flux from the nearest known Gaia EDR3 and TIC neighbor (TIC 724109412) $25''.4$ Southwest. We detect the transit event within the TOI-904 photometric apertures in the two *z*-short band light curves and include the data in the analyses of this work (see Fig. 2).

We attempted to observe an additional transit of TOI-904 c on UTC 2022 February 27 with the South Africa Astronomical Observatory, resulting in a tentative partial transit detection. This detection, however, lacked a sufficient out-of-transit baseline to be conclusive and is not included in the analyses of this work.

2.3. Spectroscopic Follow-up

Brown dwarf or grazing stellar binaries are frequent sources of false positive transit signals. While few instru-

³ <https://exofop.ipac.caltech.edu/tess/target.php?id=261257684>

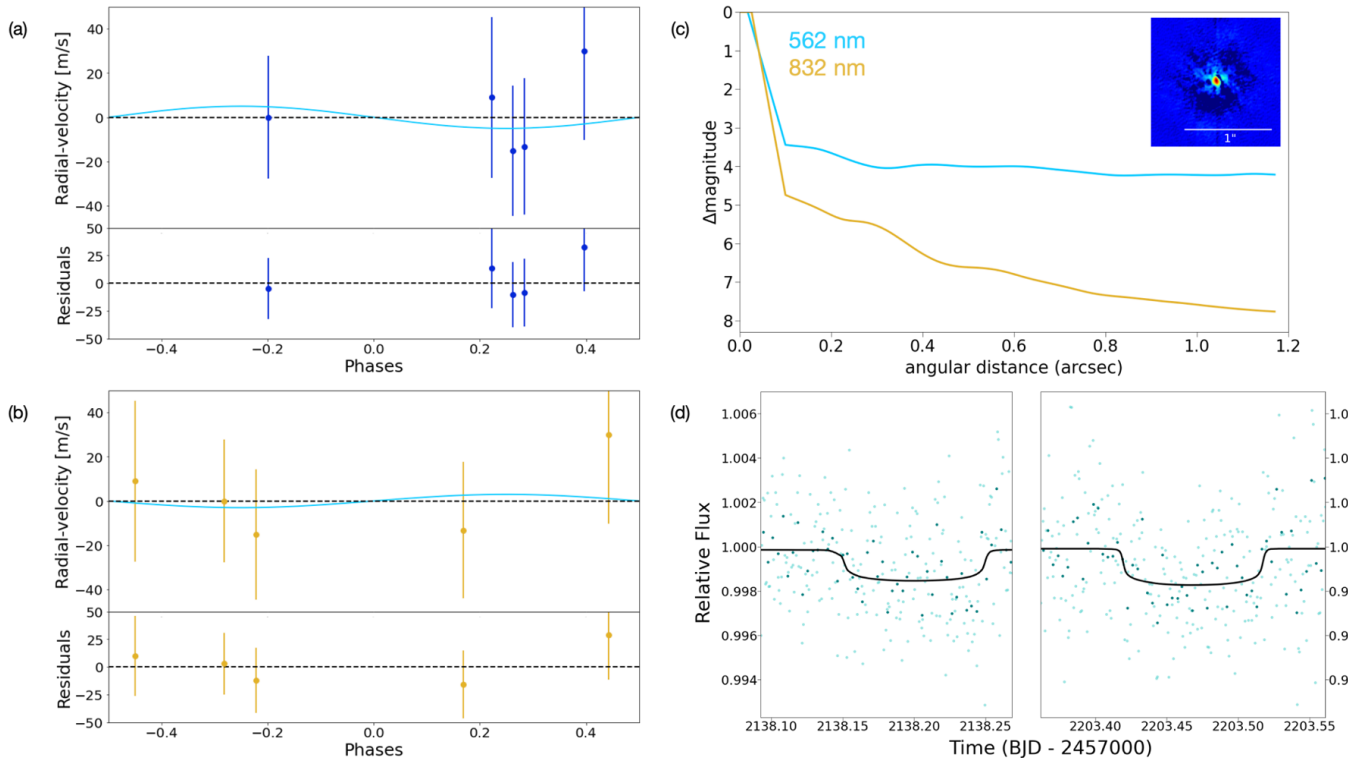


Figure 2. Follow-up observations of the planetary system around TOI-904. **Left:** CORALIE observations phase-folded on the periods of both TOI-904 b (**Panel (a)**, dark blue) and TOI-904 c (**Panel (b)**, gold). The best fit radial velocity trends for both phase-folded data sets are shown in light blue. Neither figure shows evidence of a stellar or brown dwarf mass companion. **Panel (c):** high-resolution imaging taken at 562 nm and 832 nm (blue and gold, respectively). There is no clear flux from another object between 0.1 and 1.2 arcsec down to 4 and 8 magnitude differences, respectively, and thus no evidence of a blending or binary star. **Panel (d):** Ground based photometric observations of TOI-904 b taken with the LCOGT Siding Spring Observatory (**Panel (d) left**) and the South Africa Astronomical Observatory (**Panel (d) right**). Observations were taken in 36 second intervals (light blue) and were binned to 5 minutes (dark blue). The best-fit transit model is overlaid in black, showing that both observations recover full transits of the planet at a comparable depth to the *TESS* observations.

ments are capable of confirming the exoplanet nature of transits by measuring the masses of small extrasolar planets, many more are equipped to detect the Doppler signal caused by a stellar or brown dwarf mass companion. Reconnaissance radial velocity measurements of the host star are thus able to rule out a false positive due to a bound stellar (or brown dwarf) binary while also providing key observations to refine the spectroscopic parameters of the host star.

2.3.1. SMARTS/CHIRON Spectroscopy

We obtained four observations of TOI-904 with the CHIRON facility on the SMARTS 1.5-meter telescope at Cerro Tololo Inter-American Observatory, Chile (Tokovinin et al. 2013). CHIRON is a high resolution spectrograph with a resolving power of $R = 80,000$ over the wavelength range of 4100–8700 Å with ‘slicer’ mode observations. The spectra were extracted via the standard pipeline as per Paredes et al. (2021).

We attempted to derive a line broadening velocity from the CHIRON observations. We performed a least-

squares deconvolution between each spectrum and a non-rotating synthetic spectrum generated via the ATLAS9 model atmospheres grid (Castelli & Kurucz 2004) at the stellar effective temperature and surface gravity of our target star. We then modeled the line broadening profile via a combination of the rotational, radial-tangential macroturbulent, and instrumental broadening kernels (as per Gray & Corbally 1994). We find the rotational broadening component to have width of $< 2 \text{ km s}^{-1}$ (1σ) when the additional broadening terms are considered, consistent with expectations from the photometric modulation derived rotation period of the target star.

2.3.2. EULER/CORALIE Spectroscopy

TOI-904 was observed by the Swiss 1.2m Euler telescope with the CORALIE instrument installed at its Nasmyth focus. CORALIE is a fiber-fed high-resolution spectrograph with a spectral resolution of 60,000 (Queloz et al. 2001). CORALIE has a 3 pixel sampling per resolution element. Five spectra of TOI-

904 were taken between 2020 February 2 and April 14 (see Figure 2). The observations have an exposure time of 2400s and reach a signal-to-noise ratio varying between 11 and 16. The observations are targeting the extreme phases of the estimated radial velocity signal (see Fig. 2 Panels a and b). The radial velocity is extracted by cross-correlating a M2 stellar mask with each spectrum (Pepe et al. 2002). The radial velocity data has an RMS of 15 m/s over the time span of the observations.

2.4. High Angular Resolution Imaging

Close stellar companions (bound or line of sight) can confound exoplanet discoveries in a number of ways. The detected transit signal might be a false positive due to a background eclipsing binary and even real planet discoveries will yield incorrect stellar and exoplanet parameters if a close companion exists and is unaccounted for (Furlan & Howell 2017, 2020). Additionally, the presence of a bound companion star leads to the non-detection of small planets residing with the same exoplanetary system (Lester et al. 2021).

2.4.1. SOAR/HRCAM High-Resolution Imaging

We searched for stellar companions to TOI-904 with speckle imaging on the 4.1-m Southern Astrophysical Research (SOAR) telescope (Tokovinin 2018) on 2022 January 07 UT, observing in Cousins I-band, a similar visible bandpass as TESS. This observation was sensitive to a 5.4-magnitude fainter star at an angular distance of 1 arcsec from the target. No nearby stars were detected within 3'' of TOI-904 in the SOAR observations.

2.4.2. Gemini South/ZORRO High-Resolution Imaging

TOI-904 was observed on 2021 October 21 UT and 2022 January 13 UT using the Zorro speckle instrument on the Gemini South 8-m telescope (Scott et al. 2021; Howell & Furlan 2022). Zorro provides simultaneous speckle imaging in two bands (562nm and 832 nm) with output data products including a reconstructed image with robust contrast limits on companion detections. While both observations had consistent results that TOI-904 is a single star to within the angular and contrast levels achieved, the January 2022 observation had better seeing which led to deeper contrast levels. Seven sets of 1000 X 0.06 second images were obtained and processed in our standard reduction pipeline (Howell et al. 2011). Figure 2 Panel c shows our final contrast curves and the 832 nm reconstructed speckle image. We find that TOI-904 is a single star with no companion brighter than 5-8 magnitudes below that of the target star from the 8-m telescope diffraction limit (20 mas) out to 1.2''. At the distance of TOI-904 (d=46 pc) these

angular limits correspond to spatial limits of 0.9 to 55 AU.

3. ANALYSIS

3.1. Host Star Parameters

As an independent determination of the basic stellar parameters from those in the TESS Input Catalog (TIC; Stassun et al. 2019), we performed an analysis of the broadband spectral energy distribution (SED) of the star together with the Gaia EDR3 (Gaia Collaboration et al. 2016, 2018) parallax (with no systematic offset applied; see, e.g., Stassun & Torres 2021), in order to determine an empirical measurement of the stellar radius, following the procedures described in Stassun & Torres (2016); Stassun et al. (2017, 2018). We pulled the JHK_S magnitudes from 2MASS (Skrutskie et al. 2006), the W1-W4 magnitudes from WISE (Wright et al. 2010), the $G_{BP}G_{RP}$ magnitudes from Gaia (Riello et al. 2021) and the NUV flux from GALEX (Martin et al. 2003, 2005). Together, the available photometry spans the stellar SED over the wavelength range 0.2–22 μm .

We performed a fit using NextGen stellar atmosphere models, with the effective temperature (T_{eff}) and metallicity ([Fe/H]) adopted from the spectroscopic analysis using the SpecMatch-Emp software tool (Yee et al. 2017) on the CORALIE spectra (the surface gravity, $\log g$, has very little influence on the broadband SED). We limited the extinction, A_V , to the full line-of-sight value from the Galactic dust maps of Schlegel et al. (1998). The resulting fit has a reduced χ^2 of 2.3 (not including the NUV flux which suggests the presence of chromospheric activity), with best-fit $A_V = 0.03 \pm 0.03$. Integrating the model SED gives the bolometric flux at Earth, $F_{\text{bol}} = 7.62 \pm 0.45 \times 10^{-10} \text{ erg s}^{-1} \text{ cm}^{-2}$. Taking the F_{bol} together with the Gaia parallax gives the stellar radius, $R_* = 0.527 \pm 0.021 R_{\odot}$. The stellar mass can also be estimated via the empirical M_K based relations of Mann et al. (2019), giving $M_* = 0.557 \pm 0.028 M_{\odot}$.

Finally, we can use the star's rotation period, P_{rot} , to estimate its age via empirical gyrochronology relations. We use the full TESS light curve and a Lomb-Scargle periodogram as implemented in astropy (Press & Rybicki 1989) to obtain a rotation period of 8.55 days, with a False Alarm Probability on the order of 10^{-181} . However, similar spot coverage on opposite hemispheres can cause aliasing at half the true rotation period, meaning the real rotation period could be 17.1 days. If in fact the period is 8.55 d, then using empirical relations for M-dwarfs from Engle & Guinan (2018), this suggests that the stellar age is approximately 1 Gyr. This relatively young age would be consistent with chromospheric ac-

Stellar Parameters		Planet Parameters		
<i>Catalogue Data</i> [†]		<i>Model Properties</i>		
TIC ID	261257684	<i>Fixed Initial Parameters</i>		
TOI	904	$q_{1,TESS}^*$	0.336	
R.A.	05:57:29.11	$q_{2,TESS}^*$	0.208	
Dec	-83:07:47.02	$q_{1,zs}^*$	0.281	
pmRA (mas yr ⁻¹)	-28.941 ± 0.032	$q_{2,zs}^*$	0.192	
pmDec (mas yr ⁻¹)	110.858 ± 0.033	eccentricity	0.0	
Parallax (mas)	21.697 ± 0.016	ω (deg)	90.0	
Distance (pc)	46.089 ± 0.035	Dilution [†]	0.994	
<i>Photometric Properties</i> [†]		<i>Modeled Parameters (SPOC individual fits)</i> [◊]		
TESS mag	10.846 ± 0.007	T0 (BJD-TDB)	2366.621 ^{+0.001} _{-0.002}	2386.349 ^{+0.003} _{-0.004}
GAIA mag	11.8559 ± 0.0004	Period (days)	10.8772 ^{+0.0003} _{-0.0003}	83.9997 ^{+0.0006} _{-0.0007}
V mag	12.588 ± 0.069	R_p/R_*	0.039 ^{+0.001} _{-0.001}	0.038 ^{+0.001} _{-0.001}
J mag	9.607 ± 0.022	ρ_* (cgs)	1.878 ^{+2.710} _{-0.960}	5.545 ^{+1.304} _{-2.535}
K mag	8.766 ± 0.021	i (deg)	88.19 ^{+1.26} _{-0.876}	89.83 ^{+0.13} _{-0.20}
<i>Stellar Properties</i>		<i>Derived Properties</i>		
M_* (M _⊙)	0.557 ± 0.028	R_p (R _⊕)	2.426 ^{+0.163} _{-0.152}	2.167 ^{+0.130} _{-0.118}
R_* (R _⊙)	0.527 ± 0.021	R_*/a	0.043 ^{+0.015} _{-0.009}	0.0078 ^{+0.0005} _{-0.0014}
L_* (L _⊙)	0.051 ± 0.012	a (AU)	0.056 ^{+0.019} _{-0.012}	0.312 ^{+0.023} _{-0.058}
ρ_* [◊] (cgs)	5.360 ± 0.296	b	0.714 ^{+0.124} _{-0.422}	0.373 ^{+0.288} _{-0.280}
T_{eff} [‡] (K)	3770.2 ± 70.0	$t_{duration}$ (hours)	3.65 ^{+1.27} _{-0.78}	5.04 ^{+0.37} _{-0.93}
[Fe/H] [‡] (dex)	0.022 ± 0.090	T_{eq} (K)	429.43 ± 32.61	217.26 ± 9.10
$v \sin i^{\boxtimes}$ (km s ⁻¹)	< 2			
Age [•] (Gyr)	1.5 ± 0.2 (or 0.8 ± 0.1)			

Table 1. Table of TOI-904 stellar parameters as well as the fitted and derived parameters of TOI-904 b and c.

†: Taken from TESS Input Catalog (Stassun et al. 2019).

‡: Derived from CORALIE observations (section 2.3.2) using SpecMatch-Emp (Yee et al. 2017).

⊗ Derived from CHIRON observations discussed in Section 2.3.1

*: Calculated using LDK (Parviainen & Aigrain 2015; Husser et al. 2013).

◊: Calculated using juliet (Espinoza et al. 2019) on SPOC (Jenkins et al. 2016) observations.

•: Section 3.1 analysis.

tivity suggested by the NUV flux in the SED, however our current constraints on $v \sin i$ from radial velocity observations of this target favor the 17.1 day period. Precise characterization of the star’s $v \sin i$ and other activity indicators such as $\log R'_{HK}$ is needed to better constrain the age of the host star.

These and additional stellar parameters are shown in Table 1.

3.2. Planet Validation

In this section we discuss and rule out false-positive scenarios that could explain the transit signals we have detected in our observations of TOI-904. Our radial velocity observations taken with the CORALIE instrument sampled the expected times of radial velocity max-

ima and minima for both planets and detected no signal indicating a stellar or brown dwarf mass companion to the host star. Using the `radvel` package (Fulton et al. 2018) under the assumption of circular orbits, we obtain 3σ mass limits of $238.85 M_{\oplus}$ and $350.34 M_{\oplus}$ for TOI-904 b and c, respectively, which precludes a stellar mass object at these orbital periods. The high angular resolution images of TOI-904 taken with SOAR and ZORRO show no nearby stars brighter than 5-8 magnitudes less than the host star to distances as close as 0.9 AU, from which we can rule out the possibilities that the transits are located on a nearby star or that a nearby star is diluting our observations. Together, the reconnaissance radial velocities and imaging observations lead us to rule

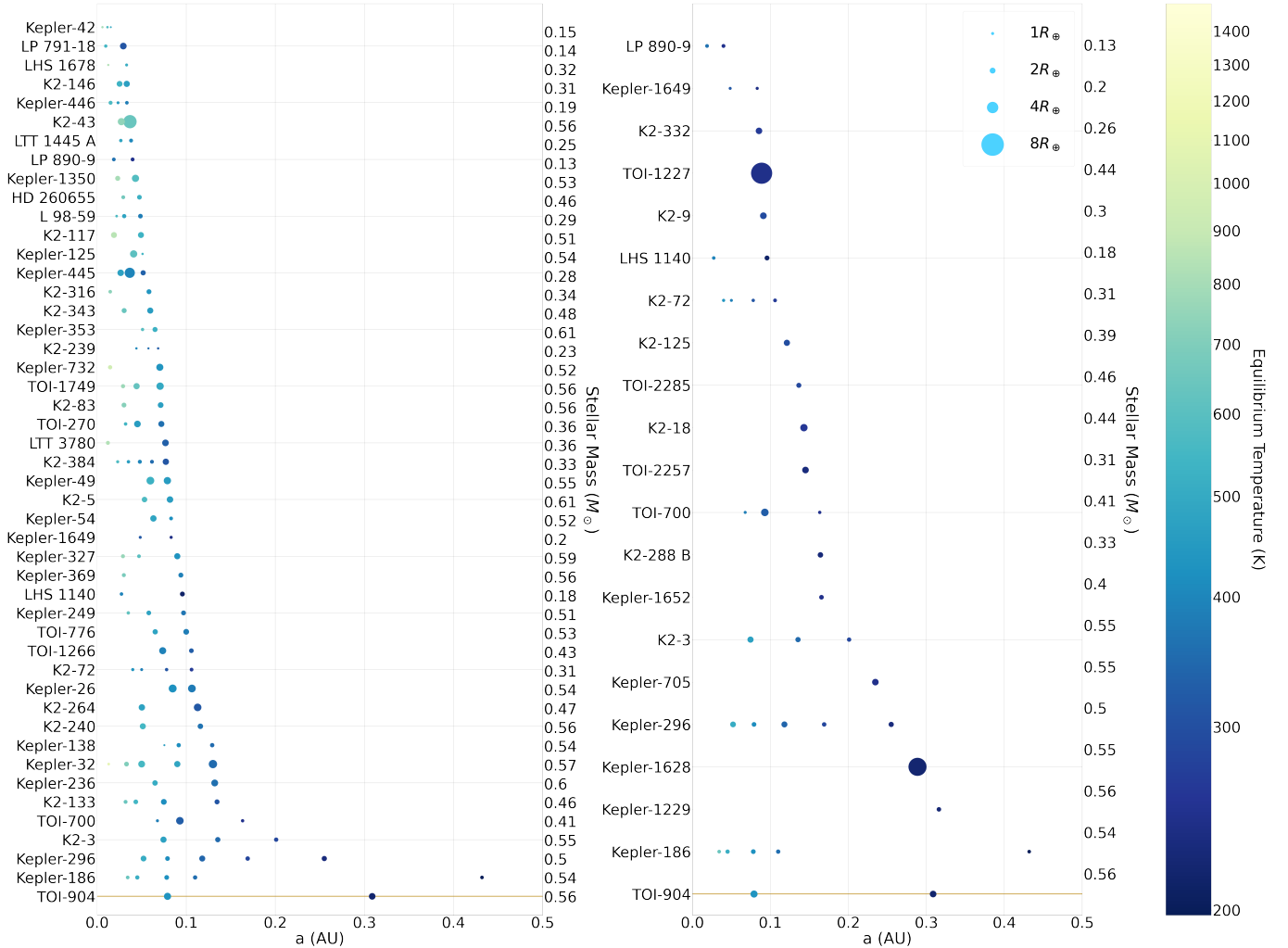


Figure 3. Plots of all known transiting multi-planet systems (**Left**) and cold planets (**Right**; $T_{eq} < 300$ K) around M dwarf stars. Each system is shown as a function of system name (left y-axis), stellar mass (right y-axis), semi-major axis (x-axis) planet equilibrium temperature (color) and planet radius (point size). TOI-904 is shown at the bottom of each panel with a gold horizontal line.

out the possibility that a blended eclipsing binary could be causing either of the observed transiting planet candidates.

Our ground-based photometric observations of TOI-904 b further allow us to eliminate the possibility that the *TESS* observations of TOI-904 b occurred on another star in the *TESS* pixel. Both observed transits had a strong significance of detection of 11σ (see Figure 2 Panel d). Although we have yet to recover a complete transit of TOI-904 c from ground-based instruments, statistical analyses from the Kepler survey (Lissauer et al. 2012; Rowe et al. 2014; Morton et al. 2016) and recent calculations based on *TESS* observations from Guerrero et al. (2021) indicate that multi-planet transiting systems are nearly always true planets, especially those with planets smaller than $6R_{\oplus}$, adding validity to the planetary nature of TOI-904 c.

Finally, we used the *triceratops* (Giacalone & Dressing 2020) software library to statistically validate both planet candidates. *triceratops* begins by using the MAST module of *astroquery* (Ginsburg et al. 2019) to obtain the TIC properties for each star within 10 pixels of the target star. Using the *TESS* magnitudes, each neighboring star is considered for its flux contribution in the target pixel and as a possible source of the transit signal. The tool then creates models of transiting planet and eclipsing binary light curves which are used to calculate the probability of each scenario using a Bayesian framework. These probabilities are then used to determine whether or not a planet candidate can be classified as “validated” (has a False Positive Probability $< 1.5\%$ and Nearby False Positive Probability $< 0.1\%$). Previously, in their work statistically validating several hundred TOIs, Giacalone & Dressing (2020) found the False Positive Probability (FPP; defined as the summed

probability of all scenarios in which a planet sized object is located on the give host star subtracted from unity) for TOI-904 b to be 3%, and designated the planet as a “Likely Planet”. By doing a joint fit using the new Gemini South/ZORRO observations discussed in Section 2.4 and incorporating all *TESS* transit detections of both planets, we find that for TOI-904 b, 3σ upper limit on the FPP = 0.049%. Doing the same calculation for TOI-904 c, we calculate the 3σ upper limit to be 0.0011%, allowing us to statistically validate both planets with >99% certainty. With the added validity from the planet multiplicity of this system (Lissauer et al. 2012), we can confidently state that both objects observed around this star are planets.

3.3. Fitting Planet Parameters

We conducted our analysis on the raw 2-minute Simple Aperture Photometry (SAP) light curves produced by the SPOC pipeline (Twicken et al. 2010; Morris et al. 2020). We obtained all available data using the Mikulski Archive for Space Telescope (MAST) portal. We removed long-timescale correlated noise (caused by stellar variability) by applying the *wotan* software library’s Tukey biweight algorithm (Hippke et al. 2019) to each sector of *TESS* observations after masking known transit signals. To conduct a transit analysis of both signals in each light curve, we use the *juliet* software library (Espinoza et al. 2019) built on the *batman* (Kreidberg 2015) transit modeling software and the *dynesty* (Speagle 2020) nested sampling algorithm for calculating Bayesian posteriors and evidences. We used the LDTK (Parviainen & Aigrain 2015; Husser et al. 2013) software to calculate the limb-darkening parameters in the *TESS* passband based on the stellar properties given in Table 1. We assumed linear ephemerides, circular orbits, and quadratic limb-darkening while fitting the following parameters: R_p/R_* , b , T_0 , P and the stellar density ρ_* . We performed both a joint multi-planet fit and individual fits for each planet (in which we masked out all transits of the other planet). We also did an independent check of the *juliet* individual planet fit analyses using the *batman* modeling package with the *emcee* (Foreman-Mackey et al. 2021) python package. The *emcee* software was used to perform an invariant Markov chain Monte Carlo (MCMC) sampling, initializing 100 walkers and having each fit take 10,000 steps with 8,000 burn-in steps. Using the same limb-darkening values, we fitted the parameters T_0 , $P, R_p/R_*$, $\cos i$ and a/R_* . Our single-planet analysis was consistent with the results from the *juliet* analysis (see Appendix A: Table 2).

As an additional cross check, we repeated this analysis for light curves produced by different pipelines to check if the transit signals were not affected by different methods of aperture selection and background subtraction. We repeated our analysis for the 30-minute light curves created by the *TESS*-SPOC, QLP and *eleanor* (Feinstein et al. 2019) pipelines (see Appendix A). As with the 2-minute observations, we used the raw undetrended data before repeating the analysis detailed above using the *emcee* and *juliet* single and multi-planet fits. We found that the transit fits created from the *eleanor*, QLP, 2-minute and 30-minute SPOC data were in agreement within 1σ .

We fit the LCO observations described in Section 2.2.1 of TOI-904 b using the *juliet* software library and our own *emcee* fit as described above and using LDTK package to calculate the star’s limb-darkening parameters in the *SLOAN/SDSS.z* passband. We found that the transit depths for the *TESS* were within 1σ of the fit we performed on the 2-minute SPOC data, as shown in Appendix A: Table 2.

4. DISCUSSION

In this Letter we have announced the discovery and validation of TOI-904 c, a cool sub-Neptune ($T_{eq} \approx 217.26 \pm 10.22$ K; $R_p = 2.310^{+0.155}_{-0.147} R_\oplus$; $P = 83.999 \pm 0.001$ days) that is the coldest planet discovered by *TESS* orbiting an M dwarf star to date. We also report on TOI-904 b, another sub-Neptune ($R_p = 2.490^{+0.203}_{-0.150} R_\oplus$; $P = 10.8772 \pm 0.0003$ days) located much closer to the early M dwarf host star.

M dwarfs are known to host a number of Earth to Neptune sized planets (see Figure 3). These planetary systems are generally very compact, and tend to exist within ~ 0.2 AU of their host star. By contrast, TOI-904 is an extended system with ~ 0.23 AU between the two planets. While distant planets have been found around other M dwarfs, all these planets were found either on the periphery of a compact system comprised of several other small planets (e.g. Kepler-186) or as the lone planet in their systems (e.g. Kepler-1628, Kepler-1229). As this is already a multi-planet system, we searched for indications of any other planets orbiting TOI-904 to determine if this system belongs in the former category. One way in which we looked for non-transiting planets was by searching for Transit-Timing Variations (TTVs) in the *TESS* and LCO observations of TOI-904 b and the *TESS* observations of TOI-904 c. We found that the maximum TTV amplitude of a sine wave fit with periods from 0.1-100 days to be 5-10 minutes for the inner planet and 25-30 minutes for the outer planet. We

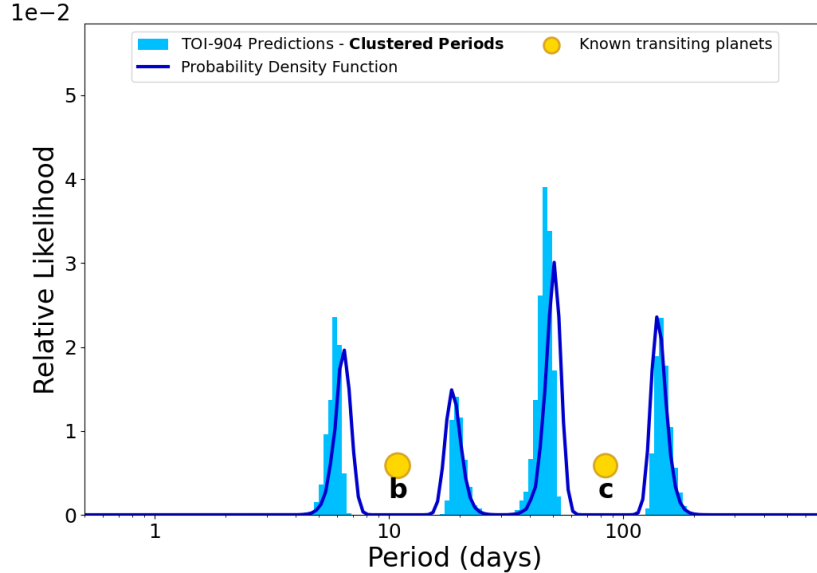


Figure 4. Created using the `dynamite` (Dietrich & Apai 2020) the relative likelihood of the most probable locations of unseen planets orbiting TOI-904 in log-period space. The yellow circle indicate the period of the two known planets in the system, while the dark blue lines show the probability density function (PDF) calculated for this system and the light blue histogram represents the stable Monte Carlo iterations sampled from the PDF. These scenarios were calculated using the `dynamite` Exoplanets Systems Simulator model (`syssim`; He et al. 2019). By incorporating the location of known planets and the stellar type, the `dynamite` software finds that additional non-transiting planets are most likely to have periods of 6.74, 18.5, 50.7, and 139.05 days.

found no current evidence of a non-transiting planet in the TTVs of the observed transits for TOI-904 b or c.

We also used the `dynamite` software library created by Dietrich & Apai (2020) to statistically calculate the potential periods and probabilities of unseen planets in multi-planet systems. `dynamite` calculates these probabilities by implementing a triple integral over the probability density function (PDF) of planet inclination, period and radius based on the occurrence rates calculated by Mulders et al. (2018), assuming each variable is independent (Dietrich & Apai 2020). This PDF is then sampled using the Monte Carlo method before producing all dynamically stable results based on calculations using Dietrich & Apai (2020) Eq. 6 (see Fig. 4). Our implementation of `dynamite` predicted four potential planets in the TOI-904 system, with orbital periods of 6.74, 18.5, 50.7, and 139.05 days (see Fig. 4). These additional planets may be detectable using extreme-precision radial velocity observations (EPRVs) or potential TTVs in future observations of TOI-904 b and c, both of which will be re-observed by TESS in sectors 65, 66 and 67.

Especially in the absence of another planet, the planets orbiting TOI-904 represent an interesting case-study for exoplanet formation scenarios around low-mass stars. TOI-904 c is one of three known transiting M dwarf planets that orbit beyond 0.2 AU and have $R_p > 1.8 R_{Earth}$, implying that they could have a gaseous enve-

lope. The other two, (Berger et al. 2018; Morton et al. 2016) however, are Kepler systems with $J_{mag} > 12$, while TOI 904 has $J_{mag} = 9.6$. This system thus provides an unprecedented opportunity to constrain planet formation at larger distances from M dwarfs by probing its atmosphere. Assuming a predicted mass of $6.1 M_{\oplus}$ (based on the mass-radius relations of Chen & Kipping 2017), the transmission spectroscopy metric (TSM; Kempton et al. 2018) of TOI-904 c is 23. Thanks mainly to its higher equilibrium temperature, the TSM of TOI-904 b (assuming a mass of $6.9 M_{\oplus}$) is 50. By comparison, the TSM values of Kepler-1628 b and Kepler-1229 b are 13 and 4, respectively.

Additional study of this system could resolve the currently ambiguous composition of the two planets. Simulations conducted by Burn et al. (2021) and Pan et al. (2022) of planet formation via core accretion around low-mass stars both predict that planets with radii $\sim 2.3 R_{\oplus}$ could have a range of densities, spanning the ultra-dense sub-Neptune, water world and puffy sub-Neptune paradigms described by Luque & Pallé (2022). Both studies expect that in any case, planets of this size are likely to have some atmosphere, so it is not realistic to expect these planets to be rocky in composition. The mass limits we obtained using `radvel` on our CORALIE measurements rule out none of these scenarios, with 2σ upper limits of 174 and $244 M_{\oplus}$ on the mass of TOI-904

b and c, respectively. With follow-up mass and atmospheric measurements, we can resolve this degeneracy for the outer planet and gain insight into planet formation of cold planets around low-mass stars. With the predicted masses mentioned above, we expect radial velocity semi-amplitude of 2.9 and 1.3 m/s for TOI-904 b and c, respectively. Based on [Luque & Pallé \(2022\)](#)'s analysis of M dwarf small planets, the three different regimes of planet density differ in scale by a factor of two (0.25, 0.5 and $1\rho_{\oplus}$ for puffy, water and rocky planets, respectively). The masses for planets in each regime would similarly differ, resulting in detectable differences in the expected semi-amplitudes of radial velocity measurements. We find that the three compositions would result in masses (semi-amplitudes) of $3.3 M_{\oplus}$ (1.4 m/s), $6.5 M_{\oplus}$ (2.9 m/s) and $13.1 M_{\oplus}$ (5.8 m/s), respectively, for the inner planet; for the outer planet, the masses (semi-amplitudes) would be $2.6 M_{\oplus}$ (1.1 m/s), $5.2 M_{\oplus}$ (2.3 m/s) and $10.4 M_{\oplus}$ (4.6 m/s), respectively. While a 5σ mass measurement ([Batalha et al. 2019](#)) could be achieved with HARPS ([Mayor et al. 2003](#)) or Magellan II/PFS ([Crane et al. 2010](#); [Teske et al. 2016](#)), particularly for TOI-904 b, the mass precision needed to distinguish between different bulk compositions is realistically only within reach of VLT-ESPRESSO ([Pepe et al. 2021](#)). Indeed, ESPRESSO was used to measure a semi-amplitude of 2.2 m/s for the candidate planet LHS 1140d, which has a period of 79 days and orbits a star five times fainter than TOI 904 ([Lillo-Box et al. 2020](#)).

If TOI-904 c is an ultra-dense Neptune, and is thus most easily detectable for mass measurements, both planets may have formed in situ ([Kennedy et al. 2006](#); [Hansen & Murray 2012](#); [Hansen 2015](#)). This case would have resulted in TOI-904 c forming as a rocky, ultra-dense Neptune (similar to K2-110 b; [Osborn et al. 2017](#)) if the snow-line of the M dwarf receded towards the star on planet formation timescales causing a late stage of mass accretion for planets located near the snow line ([Kennedy et al. 2006](#)). In situ formation seems unlikely for this system, however, as the larger inner planet TOI-904 b could not have reached its size at its current location due to the high temperature (>2000 K; [Ali-Dib et al. 2020](#)) of a forming protoplanet at this distance from the host star, precluding the accretion of any gaseous envelope. In situ formation also often predicts 4-10 rocky planets on co-planar orbits ([Hansen & Murray 2012](#); [Pan et al. 2022](#)), for which there is currently no evidence in this system.

It is more probable that TOI-904 c migrated to its current location from a greater distance via type-I migration ([Burn et al. 2021](#); [Luque & Pallé 2022](#); [Pan et al. 2022](#)). If the planet did form further in the disk, its core

was likely formed of both rock and ice materials before the planet migrated inward. In this case, this planet's density could allow us to differentiate between a 'water world' with $\sim 50\%$ ice/rock ratios and little to no envelope ([Burn et al. 2021](#); [Luque & Pallé 2022](#)) and a planet with a lower ice/rock ratio and a larger atmosphere ([Pan et al. 2022](#)). In this model, the inner planet's core could be made up of rocky materials or an ice/rock mixture. If the latter, [Bitsch et al. \(2019\)](#) state that the hot inner water world would be considerable evidence for the planet migration model, and TOI-904 b's overall water content could inform the exact migration history of that planet. If instead planet b has a large gaseous envelope, its water content could still inform which formation path this system followed and where it acquired its envelope, either as it did so beyond the snow line ([Burn et al. 2021](#)) or after being trapped in inner regions of the protoplanetary disk, where little water is available to accrete ([Pan et al. 2022](#)).

Type-I migration is a very efficient process, however, and models of this theory predict very compact multi-planet systems, unlike the widely separated planets orbiting TOI-904. One possibility to resolve this discrepancy is that TOI-904 c formed at a significantly greater distance from the host star than TOI-904 b, which would explain why the inner planet migrated in so much further and why the mutual separation of the planets has persisted. This could also result from lower disk density at greater distances, where type-I migration could be triggered for smaller planets like TOI-904 c ([Burn et al. 2021](#)). This theory could be tested by determining if TOI-904 c has a larger C/O ratio than TOI-904 b, which would indicate that TOI-904 c may have formed beyond the methane ice line and that TOI-904 b did not.

Given that the planets are so similar in size, a final alternate theory could be that they followed the same formation path by forming sequentially, following the inside-out formation theory suggested by [Chatterjee & Tan \(2014\)](#). In this theory, pebbles form in outer regions of this disk before migrating inward and stalling at a high pressure region (potentially at the water ice line) before forming a planet at that location. The planet would then migrate inward and cause the high pressure zone to move outward, allowing the process to repeat and form another planet. [Pan et al. \(2022\)](#) conducted the first simulations of this type of formation around M dwarfs, and found that it is likely to result in systems of 2-4 sub-Neptune sized planets located at greater distances and separations than type-I migration would produce, and thus more closely resemble the TOI-904 system. If both planets have a high water content,

TOI-904 b’s larger size could be explained by an inflated hydrosphere caused by its closer proximity to the star (Luque et al. 2019). If the compositions of these planets are similar, the TOI-904 system could strongly support this relatively new theory of planet formation. Whatever theory of formation dominates in these systems, through investigating the mass and atmospheric composition of both planets we can determine whether they have twin compositions or are only sibling planets orbiting the same star.

ACKNOWLEDGEMENTS

Facilities: LCOGT, Gemini South/ZORRO, EULER/CORALIE, SOAR/HRCAM

Software: AstroImageJ (Collins et al. 2017), TAPIR (Jensen 2013), astropy (Astropy Collaboration et al. 2013, 2018, 2022), triceratops (Giacalone & Dressing 2020), juliet (Espinoza et al. 2019), emcee (Foreman-Mackey et al. 2013), batman (Kreidberg 2015), wotan (Hippke et al. 2019), eleanor (Feinstein et al. 2019), dynesty (Speagle 2020), LDTK (Parviainen & Aigrain 2015; Husser et al. 2013), SpecMatch-Emp (Yee et al. 2017)

We thank the anonymous reviewer for their feedback and suggestions which have helped improve this paper.

We would also like to acknowledge Rebekah Dawson at the Center for Exoplanets and Habitable Worlds at Pennsylvania State University for her advice in regards to the TTV analysis conducted in this paper.

Some of the data presented in this paper were obtained from the Mikulski Archive for Space Telescopes (MAST) at the Space Telescope Science Institute. The specific observations analyzed can be accessed via DOI: [10.17909/73w3-v751](https://doi.org/10.17909/73w3-v751).

This research has made use of the NASA Exoplanet Archive, which is operated by the California Institute of Technology, under contract with the National Aeronautics and Space Administration under the Exoplanet Exploration Program. The data described here may be obtained from <https://dx.doi.org/10.17909/T9RP4V>. We acknowledge the use of public TESS data from pipelines at the TESS Science Office and at the TESS Science Processing Operations Center. Resources supporting this work were provided by the NASA High-End Computing (HEC) Program through the NASA Advanced Supercomputing (NAS) Division at Ames Research Center for the production of the SPOC data products. Some of the observations in the paper made use of the High-Resolution Imaging instrument Zorro obtained under Gemini LLP Proposal Number: GN/S-2021A-LP-105. Zorro was funded by the NASA Exoplanet Ex-

ploration Program and built at the NASA Ames Research Center by Steve B. Howell, Nic Scott, Elliott P. Horch, and Emmett Quigley. Zorro was mounted on the Gemini North (and/or South) telescope of the international Gemini Observatory, a program of NSF’s OIR Lab, which is managed by the Association of Universities for Research in Astronomy (AURA) under a cooperative agreement with the National Science Foundation on behalf of the Gemini partnership: the National Science Foundation (United States), National Research Council (Canada), Agencia Nacional de Investigación y Desarrollo (Chile), Ministerio de Ciencia, Tecnología e Innovación (Argentina), Ministério da Ciência, Tecnologia, Inovações e Comunicações (Brazil), and Korea Astronomy and Space Science Institute (Republic of Korea). This work makes use of observations from the LCOGT network. Part of the LCOGT telescope time was granted by NOIRLab through the Mid-Scale Innovations Program (MSIP). MSIP is funded by NSF. This research has made use of the Exoplanet Follow-up Observation Program (ExoFOP⁴) website, which is operated by the California Institute of Technology, under contract with the National Aeronautics and Space Administration under the Exoplanet Exploration Program. This work was based in part on observations obtained at the Southern Astrophysical Research (SOAR) telescope, which is a joint project of the Ministério da Ciência, Tecnologia e Inovações (MCTI/LNA) do Brasil, the US National Science Foundation’s NOIRLab, the University of North Carolina at Chapel Hill (UNC), and Michigan State University (MSU). This work has made use of data from the European Space Agency (ESA) mission *Gaia* (<https://www.cosmos.esa.int/gaia>), processed by the *Gaia* Data Processing and Analysis Consortium (DPAC, <https://www.cosmos.esa.int/web/gaia/dpac/consortium>). Funding for the DPAC has been provided by national institutions, in particular the institutions participating in the *Gaia* Multilateral Agreement. This publication makes use of data products from the Two Micron All Sky Survey, which is a joint project of the University of Massachusetts and the Infrared Processing and Analysis Center/California Institute of Technology, funded by the National Aeronautics and Space Administration and the National Science Foundation. This publication makes use of data products from the Wide-field Infrared Survey Explorer, which is a joint project of the University of California, Los Angeles, and the Jet Propulsion Laboratory/California Institute of Technology, funded by the

⁴ DOI: 10.26134/ExoFOP5

National Aeronautics and Space Administration. D. D. acknowledges support from the TESS Guest Investigator Program grants 80NSSC22K0185 and , and NASA Exoplanet Research Program grant 18-2XRP18.2-0136. The contributions of S. U., M .L. and H. O. have been

carried out within the framework of the NCCR PlanetS supported by the Swiss National Science Foundation under grants 51NF40_182901 and 51NF40_205606. M. L. further acknowledges support of the Swiss National Science Foundation under grant number PCEFP2_194576.

REFERENCES

- Ali-Dib, M., Cumming, A., & Lin, D. N. C. 2020, *MNRAS*, 494, 2440, doi: [10.1093/mnras/staa914](https://doi.org/10.1093/mnras/staa914)
- Astropy Collaboration, Robitaille, T. P., Tollerud, E. J., et al. 2013, *A&A*, 558, A33, doi: [10.1051/0004-6361/201322068](https://doi.org/10.1051/0004-6361/201322068)
- Astropy Collaboration, Price-Whelan, A. M., Sipőcz, B. M., et al. 2018, *AJ*, 156, 123, doi: [10.3847/1538-3881/aabc4f](https://doi.org/10.3847/1538-3881/aabc4f)
- Astropy Collaboration, Price-Whelan, A. M., Lim, P. L., et al. 2022, *apj*, 935, 167, doi: [10.3847/1538-4357/ac7c74](https://doi.org/10.3847/1538-4357/ac7c74)
- Barclay, T., Quintana, E. V., Adams, F. C., et al. 2015, *ApJ*, 809, 7, doi: [10.1088/0004-637X/809/1/7](https://doi.org/10.1088/0004-637X/809/1/7)
- Batalha, N. E., Lewis, T., Fortney, J. J., et al. 2019, *ApJL*, 885, L25, doi: [10.3847/2041-8213/ab4909](https://doi.org/10.3847/2041-8213/ab4909)
- Berger, T. A., Huber, D., Gaidos, E., & van Saders, J. L. 2018, *ApJ*, 866, 99, doi: [10.3847/1538-4357/aada83](https://doi.org/10.3847/1538-4357/aada83)
- Bitsch, B., Raymond, S. N., & Izidoro, A. 2019, *A&A*, 624, A109, doi: [10.1051/0004-6361/201935007](https://doi.org/10.1051/0004-6361/201935007)
- Brown, T. M., Baliber, N., Bianco, F. B., et al. 2013, *PASP*, 125, 1031, doi: [10.1086/673168](https://doi.org/10.1086/673168)
- Burn, R., Schlecker, M., Mordasini, C., et al. 2021, arXiv e-prints, arXiv:2105.04596. <https://arxiv.org/abs/2105.04596>
- Cañas, C. I., Stefansson, G., Kanodia, S., et al. 2020, *AJ*, 160, 147, doi: [10.3847/1538-3881/abac67](https://doi.org/10.3847/1538-3881/abac67)
- Castelli, F., & Kurucz, R. L. 2004, ArXiv Astrophysics e-prints
- Chatterjee, S., & Tan, J. C. 2014, *ApJ*, 780, 53, doi: [10.1088/0004-637X/780/1/53](https://doi.org/10.1088/0004-637X/780/1/53)
- Chen, J., & Kipping, D. 2017, *ApJ*, 834, 17, doi: [10.3847/1538-4357/834/1/17](https://doi.org/10.3847/1538-4357/834/1/17)
- Collins, K. 2019, in American Astronomical Society Meeting Abstracts, Vol. 233, American Astronomical Society Meeting Abstracts #233, 140.05
- Collins, K. A., Kielkopf, J. F., Stassun, K. G., & Hessman, F. V. 2017, *AJ*, 153, 77, doi: [10.3847/1538-3881/153/2/77](https://doi.org/10.3847/1538-3881/153/2/77)
- Crane, J. D., Shectman, S. A., Butler, R. P., et al. 2010, in Society of Photo-Optical Instrumentation Engineers (SPIE) Conference Series, Vol. 7735, Ground-based and Airborne Instrumentation for Astronomy III, ed. I. S. McLean, S. K. Ramsay, & H. Takami, 773553, doi: [10.1117/12.857792](https://doi.org/10.1117/12.857792)
- Dietrich, J., & Apai, D. 2020, *AJ*, 160, 107, doi: [10.3847/1538-3881/aba61d](https://doi.org/10.3847/1538-3881/aba61d)
- Dressing, C. D., & Charbonneau, D. 2015, *The Astrophysical Journal*, 807, 45, doi: [10.1088/0004-637x/807/1/45](https://doi.org/10.1088/0004-637x/807/1/45)
- Engle, S. G., & Guinan, E. F. 2018, *Research Notes of the American Astronomical Society*, 2, 34, doi: [10.3847/2515-5172/aab1f8](https://doi.org/10.3847/2515-5172/aab1f8)
- Espinoza, N., Kossakowski, D., & Brahm, R. 2019, *MNRAS*, 490, 2262, doi: [10.1093/mnras/stz2688](https://doi.org/10.1093/mnras/stz2688)
- Feinstein, A. D., Montet, B. T., Foreman-Mackey, D., et al. 2019, *PASP*, 131, 094502, doi: [10.1088/1538-3873/ab291c](https://doi.org/10.1088/1538-3873/ab291c)
- Foreman-Mackey, D., Hogg, D. W., Lang, D., & Goodman, J. 2013, *PASP*, 125, 306, doi: [10.1086/670067](https://doi.org/10.1086/670067)
- Foreman-Mackey, D., Luger, R., Agol, E., et al. 2021, arXiv e-prints, arXiv:2105.01994. <https://arxiv.org/abs/2105.01994>
- Fukui, A., Kimura, T., Hirano, T., et al. 2022, *PASJ*, 74, L1, doi: [10.1093/pasj/psab106](https://doi.org/10.1093/pasj/psab106)
- Fulton, B. J., Petigura, E. A., Blunt, S., & Sinukoff, E. 2018, *PASP*, 130, 044504, doi: [10.1088/1538-3873/aaaaa8](https://doi.org/10.1088/1538-3873/aaaaa8)
- Furlan, E., & Howell, S. B. 2017, *AJ*, 154, 66, doi: [10.3847/1538-3881/aa7b70](https://doi.org/10.3847/1538-3881/aa7b70)
- . 2020, *ApJ*, 898, 47, doi: [10.3847/1538-4357/ab9c9c](https://doi.org/10.3847/1538-4357/ab9c9c)
- Gaia Collaboration, Prusti, T., de Bruijne, J. H. J., et al. 2016, *A&A*, 595, A1, doi: [10.1051/0004-6361/201629272](https://doi.org/10.1051/0004-6361/201629272)
- Gaia Collaboration, Brown, A. G. A., Vallenari, A., et al. 2018, *A&A*, 616, A1, doi: [10.1051/0004-6361/201833051](https://doi.org/10.1051/0004-6361/201833051)
- Gaia Collaboration, Vallenari, A., Brown, A. G. A., et al. 2022, arXiv e-prints, arXiv:2208.00211. <https://arxiv.org/abs/2208.00211>
- Giacalone, S., & Dressing, C. D. 2020, triceratops: Candidate exoplanet rating tool. <http://ascl.net/2002.004>
- Ginsburg, A., Sipőcz, B. M., Brasseur, C. E., et al. 2019, *AJ*, 157, 98, doi: [10.3847/1538-3881/aafc33](https://doi.org/10.3847/1538-3881/aafc33)
- Gray, R. O., & Corbally, C. J. 1994, *AJ*, 107, 742, doi: [10.1086/116893](https://doi.org/10.1086/116893)
- Guerrero, N. M., Seager, S., Huang, C. X., et al. 2021, *ApJS*, 254, 39, doi: [10.3847/1538-4365/abef1](https://doi.org/10.3847/1538-4365/abef1)
- Hansen, B. M. S. 2015, *International Journal of Astrobiology*, 14, 267, doi: [10.1017/S1473550414000159](https://doi.org/10.1017/S1473550414000159)

- Hansen, B. M. S., & Murray, N. 2012, *ApJ*, 751, 158, doi: [10.1088/0004-637X/751/2/158](https://doi.org/10.1088/0004-637X/751/2/158)
- Hardegree-Ullman, K. K., Cushing, M. C., Muirhead, P. S., & Christiansen, J. L. 2019, *AJ*, 158, 75, doi: [10.3847/1538-3881/ab21d2](https://doi.org/10.3847/1538-3881/ab21d2)
- He, M. Y., Ford, E. B., & Ragozzine, D. 2019, *MNRAS*, 490, 4575, doi: [10.1093/mnras/stz2869](https://doi.org/10.1093/mnras/stz2869)
- Hippke, M., David, T. J., Mulders, G. D., & Heller, R. 2019, *AJ*, 158, 143, doi: [10.3847/1538-3881/ab3984](https://doi.org/10.3847/1538-3881/ab3984)
- Howell, S. B., Everett, M. E., Sherry, W., Horch, E., & Ciardi, D. R. 2011, *AJ*, 142, 19, doi: [10.1088/0004-6256/142/1/19](https://doi.org/10.1088/0004-6256/142/1/19)
- Howell, S. B., & Furlan, E. 2022, *Frontiers in Astronomy and Space Sciences*, 9, 871163, doi: [10.3389/fspas.2022.871163](https://doi.org/10.3389/fspas.2022.871163)
- Husser, T.-O., Wende-von Berg, S., Dreizler, S., et al. 2013, *A&A*, 553, A6, doi: [10.1051/0004-6361/201219058](https://doi.org/10.1051/0004-6361/201219058)
- Jenkins, J. M. 2002, *ApJ*, 575, 493, doi: [10.1086/341136](https://doi.org/10.1086/341136)
- Jenkins, J. M., Tenenbaum, P., Seader, S., et al. 2020, *Kepler Data Processing Handbook: Transiting Planet Search*, Kepler Science Document KSCI-19081-003
- Jenkins, J. M., Chandrasekaran, H., McCauliff, S. D., et al. 2010, in *Society of Photo-Optical Instrumentation Engineers (SPIE) Conference Series*, Vol. 7740, *Software and Cyberinfrastructure for Astronomy*, ed. N. M. Radziwill & A. Bridger, 77400D, doi: [10.1117/12.856764](https://doi.org/10.1117/12.856764)
- Jenkins, J. M., Twicken, J. D., McCauliff, S., et al. 2016, in *Society of Photo-Optical Instrumentation Engineers (SPIE) Conference Series*, Vol. 9913, *Software and Cyberinfrastructure for Astronomy IV*, ed. G. Chiozzi & J. C. Guzman, 99133E, doi: [10.1117/12.2233418](https://doi.org/10.1117/12.2233418)
- Jensen, E. 2013, *Tapir: A web interface for transit/eclipse observability*, *Astrophysics Source Code Library*. <http://ascl.net/1306.007>
- Kempton, E. M. R., Bean, J. L., Louie, D. R., et al. 2018, *PASP*, 130, 114401, doi: [10.1088/1538-3873/aad6ff](https://doi.org/10.1088/1538-3873/aad6ff)
- Kennedy, G. M., Kenyon, S. J., & Bromley, B. C. 2006, *ApJL*, 650, L139, doi: [10.1086/508882](https://doi.org/10.1086/508882)
- Kreidberg, L. 2015, *PASP*, 127, 1161, doi: [10.1086/683602](https://doi.org/10.1086/683602)
- Kristiansen, M. H. K., Rappaport, S. A., Vanderburg, A. M., et al. 2022, *PASP*, 134, 074401, doi: [10.1088/1538-3873/ac6e06](https://doi.org/10.1088/1538-3873/ac6e06)
- Lester, K. V., Matson, R. A., Howell, S. B., et al. 2021, *AJ*, 162, 75, doi: [10.3847/1538-3881/ac0d06](https://doi.org/10.3847/1538-3881/ac0d06)
- Li, J., Tenenbaum, P., Twicken, J. D., et al. 2019, *PASP*, 131, 024506, doi: [10.1088/1538-3873/aaf44d](https://doi.org/10.1088/1538-3873/aaf44d)
- Lillo-Box, J., Figueira, P., Leleu, A., et al. 2020, *A&A*, 642, A121, doi: [10.1051/0004-6361/202038922](https://doi.org/10.1051/0004-6361/202038922)
- Lindgren, L., Hernández, J., Bombrun, A., et al. 2018, *A&A*, 616, A2, doi: [10.1051/0004-6361/201832727](https://doi.org/10.1051/0004-6361/201832727)
- Lissauer, J. J., Marcy, G. W., Rowe, J. F., et al. 2012, *ApJ*, 750, 112, doi: [10.1088/0004-637X/750/2/112](https://doi.org/10.1088/0004-637X/750/2/112)
- Luque, R., & Pallé, E. 2022, *Science*, 377, 1211, doi: [10.1126/science.abl7164](https://doi.org/10.1126/science.abl7164)
- Luque, R., Pallé, E., Kossakowski, D., et al. 2019, *A&A*, 628, A39, doi: [10.1051/0004-6361/201935801](https://doi.org/10.1051/0004-6361/201935801)
- Mann, A. W., Dupuy, T., Kraus, A. L., et al. 2019, *ApJ*, 871, 63, doi: [10.3847/1538-4357/aaf3bc](https://doi.org/10.3847/1538-4357/aaf3bc)
- Mann, A. W., Wood, M. L., Schmidt, S. P., et al. 2022, *AJ*, 163, 156, doi: [10.3847/1538-3881/ac511d](https://doi.org/10.3847/1538-3881/ac511d)
- Martin, C., Barlow, T., Barnhart, W., et al. 2003, in *Society of Photo-Optical Instrumentation Engineers (SPIE) Conference Series*, Vol. 4854, *Future EUV/UV and Visible Space Astrophysics Missions and Instrumentation*, ed. J. C. Blades & O. H. W. Siegmund, 336–350, doi: [10.1117/12.460034](https://doi.org/10.1117/12.460034)
- Martin, D. C., Fanson, J., Schiminovich, D., et al. 2005, *ApJL*, 619, L1, doi: [10.1086/426387](https://doi.org/10.1086/426387)
- Mayor, M., Pepe, F., Queloz, D., et al. 2003, *The Messenger*, 114, 20
- McCully, C., Volgenau, N. H., Harbeck, D.-R., et al. 2018, in *Society of Photo-Optical Instrumentation Engineers (SPIE) Conference Series*, Vol. 10707, *Proc. SPIE*, 107070K, doi: [10.1117/12.2314340](https://doi.org/10.1117/12.2314340)
- Morris, R. L., Twicken, J. D., Smith, J. C., et al. 2020, *Kepler Data Processing Handbook: Photometric Analysis*, Kepler Science Document KSCI-19081-003
- Morton, T. D., Bryson, S. T., Coughlin, J. L., et al. 2016, *ApJ*, 822, 86, doi: [10.3847/0004-637X/822/2/86](https://doi.org/10.3847/0004-637X/822/2/86)
- Muirhead, P. S., Hamren, K., Schlawin, E., et al. 2012, *ApJL*, 750, L37, doi: [10.1088/2041-8205/750/2/L37](https://doi.org/10.1088/2041-8205/750/2/L37)
- Mulders, G. D., Pascucci, I., Apai, D., & Ciesla, F. J. 2018, *AJ*, 156, 24, doi: [10.3847/1538-3881/aac5ea](https://doi.org/10.3847/1538-3881/aac5ea)
- Osborn, H. P., Santerne, A., Barros, S. C. C., et al. 2017, *A&A*, 604, A19, doi: [10.1051/0004-6361/201628932](https://doi.org/10.1051/0004-6361/201628932)
- Pan, M., Wang, S., & Ji, J. 2022, *MNRAS*, 510, 4134, doi: [10.1093/mnras/stab3611](https://doi.org/10.1093/mnras/stab3611)
- Paredes, L. A., Henry, T. J., Quinn, S. N., et al. 2021, *AJ*, 162, 176, doi: [10.3847/1538-3881/ac082a](https://doi.org/10.3847/1538-3881/ac082a)
- Parviainen, H., & Aigrain, S. 2015, *MNRAS*, 453, 3821, doi: [10.1093/mnras/stv1857](https://doi.org/10.1093/mnras/stv1857)
- Pearce, L. A., Kraus, A. L., Dupuy, T. J., et al. 2020, *ApJ*, 894, 115, doi: [10.3847/1538-4357/ab8389](https://doi.org/10.3847/1538-4357/ab8389)
- Pepe, F., Mayor, M., Rupprecht, G., et al. 2002, *The Messenger*, 110, 9
- Pepe, F., Cristiani, S., Rebolo, R., et al. 2021, *A&A*, 645, A96, doi: [10.1051/0004-6361/202038306](https://doi.org/10.1051/0004-6361/202038306)
- Press, W. H., & Rybicki, G. B. 1989, *ApJ*, 338, 277, doi: [10.1086/167197](https://doi.org/10.1086/167197)

- Queloz, D., Mayor, M., Udry, S., et al. 2001, *The Messenger*, 105, 1
- Quintana, E. V., Barclay, T., Raymond, S. N., et al. 2014, *Science*, 344, 277, doi: [10.1126/science.1249403](https://doi.org/10.1126/science.1249403)
- Ricker, G. R., Winn, J. N., Vanderspek, R., et al. 2015, *Journal of Astronomical Telescopes, Instruments, and Systems*, 1, 014003, doi: [10.1117/1.JATIS.1.1.014003](https://doi.org/10.1117/1.JATIS.1.1.014003)
- Riello, M., De Angeli, F., Evans, D. W., et al. 2021, *A&A*, 649, A3, doi: [10.1051/0004-6361/202039587](https://doi.org/10.1051/0004-6361/202039587)
- Rodriguez, J. E., Vanderburg, A., Zieba, S., et al. 2020, arXiv e-prints, arXiv:2001.00954, <https://arxiv.org/abs/2001.00954>
- Rowe, J. F., Bryson, S. T., Marcy, G. W., et al. 2014, *ApJ*, 784, 45, doi: [10.1088/0004-637X/784/1/45](https://doi.org/10.1088/0004-637X/784/1/45)
- Schanche, N., Pozuelos, F. J., Günther, M. N., et al. 2022, *A&A*, 657, A45, doi: [10.1051/0004-6361/202142280](https://doi.org/10.1051/0004-6361/202142280)
- Schlegel, D. J., Finkbeiner, D. P., & Davis, M. 1998, *ApJ*, 500, 525, doi: [10.1086/305772](https://doi.org/10.1086/305772)
- Scott, N. J., Howell, S. B., Gnilka, C. L., et al. 2021, *Frontiers in Astronomy and Space Sciences*, 8, 138, doi: [10.3389/fspas.2021.716560](https://doi.org/10.3389/fspas.2021.716560)
- Skrutskie, M. F., Cutri, R. M., Stiening, R., et al. 2006, *AJ*, 131, 1163, doi: [10.1086/498708](https://doi.org/10.1086/498708)
- Speagle, J. S. 2020, *MNRAS*, 493, 3132, doi: [10.1093/mnras/staa278](https://doi.org/10.1093/mnras/staa278)
- Stassun, K. G., Collins, K. A., & Gaudi, B. S. 2017, *AJ*, 153, 136, doi: [10.3847/1538-3881/aa5df3](https://doi.org/10.3847/1538-3881/aa5df3)
- Stassun, K. G., Corsaro, E., Pepper, J. A., & Gaudi, B. S. 2018, *AJ*, 155, 22, doi: [10.3847/1538-3881/aa998a](https://doi.org/10.3847/1538-3881/aa998a)
- Stassun, K. G., & Torres, G. 2016, *AJ*, 152, 180, doi: [10.3847/0004-6256/152/6/180](https://doi.org/10.3847/0004-6256/152/6/180)
- . 2021, *ApJL*, 907, L33, doi: [10.3847/2041-8213/abdaad](https://doi.org/10.3847/2041-8213/abdaad)
- Stassun, K. G., Oelkers, R. J., Paegert, M., et al. 2019, *AJ*, 158, 138, doi: [10.3847/1538-3881/ab3467](https://doi.org/10.3847/1538-3881/ab3467)
- Teske, J. K., Sheckman, S. A., Vogt, S. S., et al. 2016, *AJ*, 152, 167, doi: [10.3847/0004-6256/152/6/167](https://doi.org/10.3847/0004-6256/152/6/167)
- Tokovinin, A. 2018, *PASP*, 130, 035002, doi: [10.1088/1538-3873/aaa7d9](https://doi.org/10.1088/1538-3873/aaa7d9)
- Tokovinin, A., Fischer, D. A., Bonati, M., et al. 2013, *PASP*, 125, 1336, doi: [10.1086/674012](https://doi.org/10.1086/674012)
- Torres, G., Kipping, D. M., Fressin, F., et al. 2015, *ApJ*, 800, 99, doi: [10.1088/0004-637X/800/2/99](https://doi.org/10.1088/0004-637X/800/2/99)
- Torres, G., Kane, S. R., Rowe, J. F., et al. 2017, *AJ*, 154, 264, doi: [10.3847/1538-3881/aa984b](https://doi.org/10.3847/1538-3881/aa984b)
- Twicken, J. D., Clarke, B. D., Bryson, S. T., et al. 2010, in *Proc. SPIE*, Vol. 7740, *Software and Cyberinfrastructure for Astronomy*, 774023, doi: [10.1117/12.856790](https://doi.org/10.1117/12.856790)
- Twicken, J. D., Catanzarite, J. H., Clarke, B. D., et al. 2018, *PASP*, 130, 064502, doi: [10.1088/1538-3873/aab694](https://doi.org/10.1088/1538-3873/aab694)
- Villanueva, Steven, J., Dragomir, D., & Gaudi, B. S. 2019, *AJ*, 157, 84, doi: [10.3847/1538-3881/aaf85e](https://doi.org/10.3847/1538-3881/aaf85e)
- Wright, E. L., Eisenhardt, P. R. M., Mainzer, A. K., et al. 2010, *AJ*, 140, 1868, doi: [10.1088/0004-6256/140/6/1868](https://doi.org/10.1088/0004-6256/140/6/1868)
- Yee, S. W., Petigura, E. A., & von Braun, K. 2017, *ApJ*, 836, 77, doi: [10.3847/1538-4357/836/1/77](https://doi.org/10.3847/1538-4357/836/1/77)

APPENDIX A

	<i>Pipelines</i>	Planet b				Planet c			
		R_p/R_*	b	i (deg)	R_p (R_\oplus)	R_p/R_*	b	i (deg)	R_p (R_\oplus)
juliet	SPOC	$0.042^{+0.002}_{-0.002}$	$0.71^{+0.12}_{-0.42}$	$88.19^{+1.26}_{-0.88}$	$2.42^{+0.16}_{-0.15}$	$0.037^{+0.002}_{-0.001}$	$0.37^{+0.29}_{-0.28}$	$89.83^{+0.13}_{-0.20}$	$2.17^{+0.13}_{-0.12}$
	TESS-SPOC	$0.042^{+0.003}_{-0.002}$	$0.79^{+0.10}_{-0.24}$	$87.73^{+1.11}_{-1.17}$	$2.46^{+0.18}_{-0.17}$	$0.037^{+0.002}_{-0.002}$	$0.42^{+0.29}_{-0.31}$	$89.80^{+0.15}_{-0.23}$	$2.20^{+0.27}_{-0.18}$
	QLP	$0.037^{+0.003}_{-0.002}$	$0.49^{+0.35}_{-0.37}$	$88.94^{+0.83}_{-1.89}$	$2.15^{+0.20}_{-0.12}$	$0.036^{+0.003}_{-0.002}$	$0.57^{+0.30}_{-0.36}$	$89.70^{+0.21}_{-0.43}$	$2.07^{+0.21}_{-0.15}$
	eleanor	$0.038^{+0.003}_{-0.002}$	$0.55^{+0.31}_{-0.34}$	$88.84^{+0.78}_{-1.77}$	$2.23^{+0.22}_{-0.14}$	$0.042^{+0.005}_{-0.003}$	$0.57^{+0.32}_{-0.22}$	$89.72^{+0.12}_{-1.50}$	$2.42^{+0.33}_{-0.20}$
	LCO (10/15/2020)	$0.036^{+0.003}_{-0.003}$	$0.47^{+0.28}_{-0.30}$	$89.11^{+0.61}_{-0.97}$	$2.10^{+0.20}_{-0.19}$				
	LCO (12/19/2020)	$0.039^{+0.003}_{-0.003}$	$0.36^{+0.23}_{-0.25}$	$89.38^{+0.44}_{-0.52}$	$2.23^{+0.18}_{-0.19}$				
juliet two- planet fit	SPOC	$0.040^{+0.001}_{-0.001}$	$0.24^{+0.25}_{-0.17}$	$89.55^{+0.32}_{-0.56}$	$2.29^{+0.10}_{-0.10}$	$0.038^{+0.001}_{-0.001}$	$0.485^{+0.13}_{-0.08}$	$89.77^{+0.04}_{-0.08}$	$2.19^{+0.11}_{-0.11}$
	TESS-SPOC	$0.039^{+0.001}_{-0.001}$	$0.24^{+0.25}_{-0.17}$	$89.55^{+0.32}_{-0.56}$	$2.29^{+0.10}_{-0.11}$	$0.035^{+0.002}_{-0.001}$	$0.39^{+0.19}_{-0.19}$	$89.82^{+0.09}_{-0.11}$	$2.03^{+0.12}_{-0.12}$
	QLP	$0.038^{+0.001}_{-0.001}$	$0.21^{+0.25}_{-0.15}$	$89.61^{+0.28}_{-0.55}$	$2.19^{+0.11}_{-0.11}$	$0.034^{+0.002}_{-0.002}$	$0.44^{+0.16}_{-0.16}$	$89.79^{+0.08}_{-0.10}$	$1.96^{+0.14}_{-0.13}$
	eleanor	$0.039^{+0.003}_{-0.002}$	$0.66^{+0.15}_{-0.24}$	$88.43^{+0.76}_{-0.90}$	$2.25^{+0.17}_{-0.14}$	$0.043^{+0.004}_{-0.003}$	$0.76^{+0.11}_{-0.18}$	$89.54^{+0.16}_{-0.22}$	$2.50^{+0.23}_{-0.20}$
emcees	SPOC	$0.041^{+0.003}_{-0.002}$	$0.65^{+0.18}_{-0.43}$	$88.48^{+1.11}_{-1.11}$	$2.38^{+0.20}_{-0.15}$	$0.037^{+0.002}_{-0.001}$	$0.35^{+0.26}_{-0.24}$	$89.84^{+0.11}_{-0.17}$	$2.14^{+0.19}_{-0.10}$
	TESS-SPOC	$0.040^{+0.002}_{-0.001}$	$0.46^{+0.31}_{-0.31}$	$89.09^{+0.65}_{-1.19}$	$2.34^{+0.17}_{-0.12}$	$0.037^{+0.002}_{-0.002}$	$0.43^{+0.30}_{-0.29}$	$89.81^{+0.13}_{-0.24}$	$2.14^{+0.15}_{-0.13}$
	QLP	$0.039^{+0.003}_{-0.002}$	$0.47^{+0.31}_{-0.32}$	$89.02^{+0.69}_{-1.31}$	$2.25^{+0.17}_{-0.13}$	$0.036^{+0.003}_{-0.002}$	$0.48^{+0.34}_{-0.33}$	$89.77^{+0.16}_{-0.36}$	$2.07^{+0.19}_{-0.15}$
	eleanor	$0.040^{+0.003}_{-0.002}$	$0.49^{+0.31}_{-0.34}$	$88.96^{+0.74}_{-1.44}$	$2.32^{+0.19}_{-0.16}$	$0.043^{+0.003}_{-0.002}$	$0.48^{+0.31}_{-0.32}$	$89.76^{+0.17}_{-0.33}$	$2.47^{+0.20}_{-0.16}$
	LCO Transits (joint fit)	$0.037^{+0.003}_{-0.004}$	$0.46^{+0.31}_{-0.31}$	$89.16^{+0.59}_{-1.21}$	$2.14^{+0.19}_{-0.25}$				

Table 2. Parameters derived from the *juliet*, *emcee* and joint *juliet* planet fits for each pipelines' data products used in this study and the LCO observations of TOI-904 b. The fits created from the **eleanor** light curves generally show a deeper transit depth the outer planet TOI-904 c. QLP light curves presented shallower transits but within an uncertainty of the SPOC and TESS-SPOC observations, as did the fits made from **eleanor** observations of the inner planet. The LCO observations both show the inner planet to be smaller than expected, and very comparable with the TESS-found sizes of the outer planet. Ground-based observations of TOI-904 c are needed to further elucidate the difference in the two planets' radii.

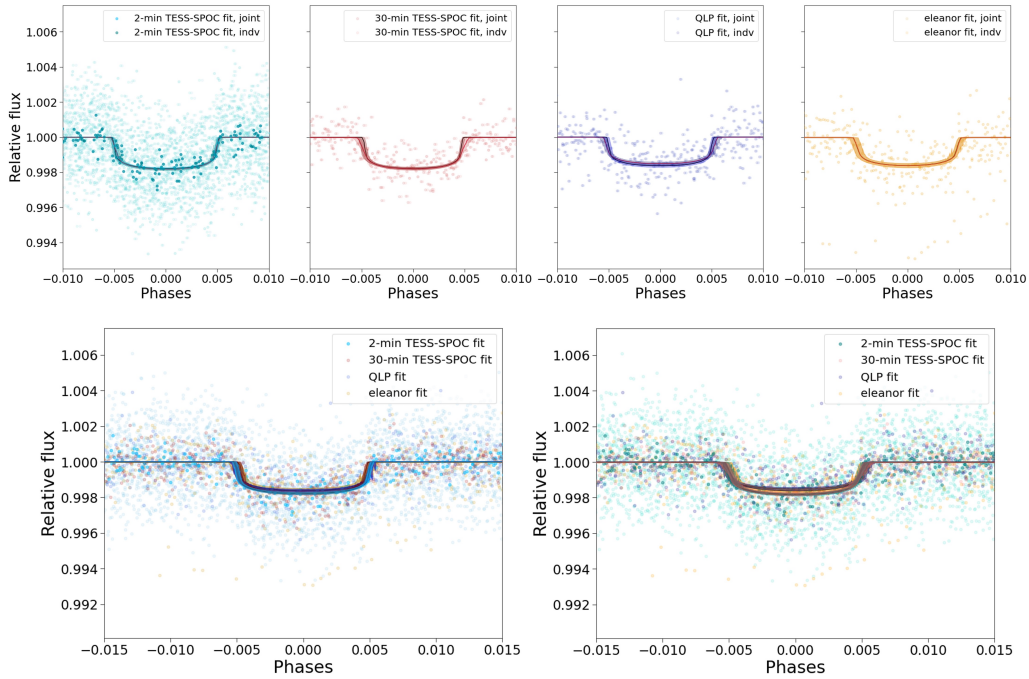


Figure 5. Graphic depictions of the *juliet* fits of TOI-904 created using the different pipelines' data products. **Top:** data from each pipeline (pale points, overlaid with darker points when binning was applied) with the joint and individual planet fits over-plotted. Source of data products from left to right: SPOC 2-minute pipeline, TESS-SPOC 30-minute pipeline, MIT Quicklook pipeline, *eleanor* pipeline). **Bottom Left:** Comparison of each joint planet fit of TOI-904 b created from the different pipelines, with the SPOC 2-minute data in light blue, the 30-minute TESS-SPOC data in red, the QLP data in dark blue and the *eleanor* data in yellow. **Bottom Right:** Same as Bottom Left figure for the individual planet fits of TOI-904 b.

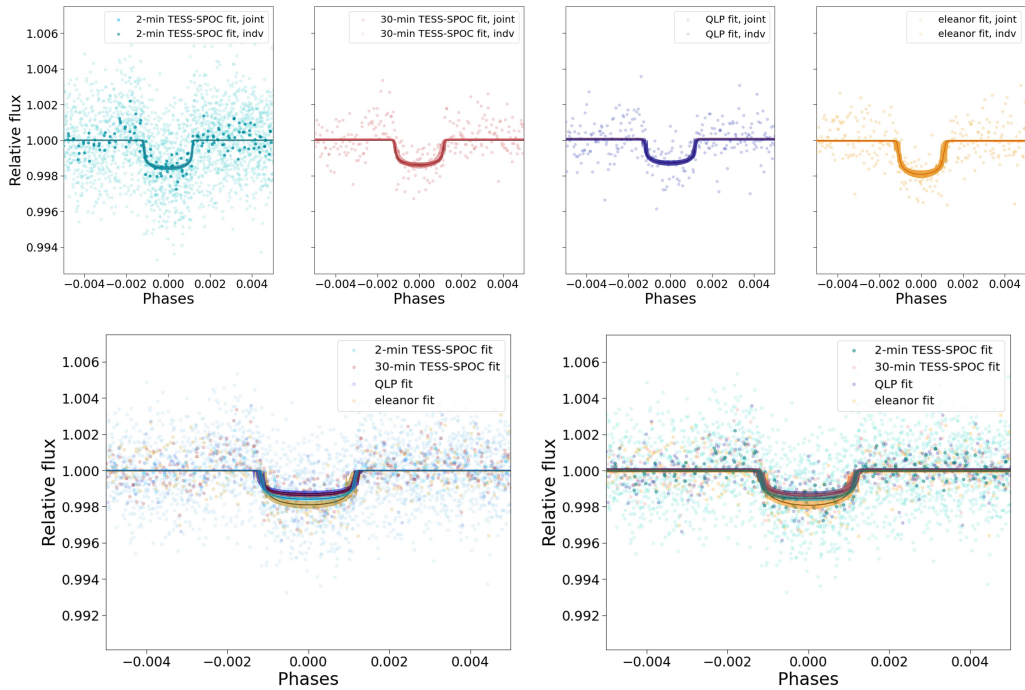


Figure 6. Same as Figure 5, fitting for TOI-904 c.

APPENDIX B

Planet	Transit Time (BJD-TDB)
TOI-904 b	$1637.847^{+0.005}_{-0.005}$
	$1648.716^{+0.006}_{-0.006}$
	$1659.599^{+0.009}_{-0.006}$
	$1670.478^{+0.009}_{-0.003}$
	$1681.374^{+0.010}_{-0.015}$
	$2040.301^{+0.003}_{-0.004}$
	$2051.181^{+0.003}_{-0.004}$
	$2344.870^{+0.003}_{-0.005}$
	$2355.746^{+0.004}_{-0.004}$
	$2366.630^{+0.006}_{-0.008}$
	$2377.510^{+0.004}_{-0.004}$
	$2388.369^{+0.006}_{-0.007}$
	$2964.869^{+0.005}_{-0.006}$
	$2986.621^{+0.005}_{-0.010}$
	TOI-904 c
$2050.349^{+0.005}_{-0.006}$	
$2386.358^{+0.006}_{-0.011}$	
$2974.345^{+0.007}_{-0.009}$	

Table 3. The transit times for all *TESS* transits of TOI-904 b and c as they were observed in Sectors 12, 13, 27, 38, 39 and 61. Two transits of TOI-904 b were excluded due to poor quality data, near 2333.999 and 2975.741.